

# $\mu$ SR study of noncentrosymmetric superconductor PbTaSe<sub>2</sub>

M.N. Wilson,<sup>1</sup> A.M. Hallas,<sup>1</sup> Y. Cai,<sup>1</sup> S. Guo,<sup>2</sup> Z. Gong,<sup>3</sup> R. Sankar,<sup>4,5</sup> F.C. Chou,<sup>4</sup> Y.J. Uemura,<sup>3</sup> and G.M. Luke<sup>1,6</sup>

<sup>1</sup>*Department of Physics and Astronomy, McMaster University, Hamilton, Ontario L8S 4M1, Canada*

<sup>2</sup>*Department of Physics, Zhejiang University, Hangzhou, China*

<sup>3</sup>*Department of Physics, Columbia University, New York, New York 10027, USA*

<sup>4</sup>*Center for Condensed Matter Sciences, National Taiwan University, Taipei 10617, Taiwan*

<sup>5</sup>*Institute of Physics, Academia Sinica, Taipei 11529, Taiwan*

<sup>6</sup>*Canadian Institute for Advanced Research, Toronto, Ontario M5G 1Z7, Canada*

We present muon spin rotation and relaxation ( $\mu$ SR) measurements on the noncentrosymmetric superconductor PbTaSe<sub>2</sub>. From measurements in an applied transverse field between  $H_{c1}$  and  $H_{c2}$ , we extract the superfluid density as a function of temperature in the vortex state. This data can be fit with a fully gapped two-band model, consistent with previous evidence from ARPES, thermal conductivity, and resistivity. Furthermore, zero field measurements show no evidence for a time reversal symmetry breaking field greater than 0.05 G in the superconducting state. This makes exotic fully gapped spin-triplet states unlikely, and hence we contend that PbTaSe<sub>2</sub> is characterized by conventional BCS s-wave superconductivity in multiple bands.

## INTRODUCTION

Noncentrosymmetric superconductors are materials where the lack of inversion symmetry gives rise to asymmetric spin-orbit coupling which splits otherwise degenerate electronic bands [1]. The broken symmetry removes means that the notion of parity can no longer be used to discuss the symmetry of a superconducting state that might emerge. This effectively allows mixed singlet and triplet states in these materials. Mixed-parity superconductivity is theoretically expected to generally give rise to nodes or partial line nodes in the gap structure [2–4].

While some noncentrosymmetric superconductors have shown evidence for line nodes, such as CePt<sub>3</sub>Si [5], CeIrSi<sub>3</sub> [6], Mg<sub>10</sub>Ir<sub>19</sub>B<sub>16</sub> [7], Mo<sub>3</sub>Al<sub>2</sub>C [8] and Li<sub>2</sub>Pt<sub>3</sub>B [9], many others display fully gapped states [10–16]. Multi-gap behavior has also been observed in materials like La<sub>2</sub>C<sub>3</sub> [17]. Detailed analysis of possible microscopic pairing mechanisms has found that either isotropic or nodal gaps can arise depending on the anisotropy of the pairing interaction [18]; this has also been suggested to depend on the spin-orbit coupling strength of the material [10]. Furthermore, even when the superconducting states appear fully gapped,  $\mu$ SR measurements have found time-reversal symmetry breaking fields in materials such as La<sub>7</sub>Ir<sub>3</sub> [13] and LaNiC<sub>2</sub> [14]. These varied properties make it valuable to study additional non-centrosymmetric systems in an effort to gain a deeper understanding of their physics.

PbTaSe<sub>2</sub> is a non-centrosymmetric material in the  $P\bar{6}m2$  space group consisting of TaSe<sub>2</sub> layers well separated by Pb interlayers, and was recently found to be superconducting with a  $T_C$  of 3.7 K [19]. This structure is similar to that of transition metal dichalcogenide (TMD) superconductors such as TaS<sub>2</sub>, IrTe<sub>2</sub> and TiSe<sub>2</sub>. In these materials, the parent compound typically hosts a charge density wave (CDW) and superconductivity emerges after the CDW is suppressed by applied pressure, doping, or intercalation [20–25]. Pure TaSe<sub>2</sub>

has a CDW [26] that is suppressed with Pb doping [27], and so we can view PbTaSe<sub>2</sub> as a stoichiometric version of the doped TMDs, deep inside the superconducting phase, with the novel feature of broken centrosymmetry. ARPES measurements have also provided evidence that the superconductivity in PbTaSe<sub>2</sub> is associated with the presence of a nearby CDW instability [28], which further strengthens the comparison between this compound and the doped TMDs.

The first studies of superconductivity in PbTaSe<sub>2</sub> indicated conventional superconductivity as the magnitude of the specific heat jump is consistent with s-wave behavior [19]. However, low temperature measurements of the upper critical field show an unconventional upward curvature [29] as a function of temperature. As  $H_{C2}(T = 0)$  is still below the Pauli limit, this has been interpreted as evidence of multi-band superconductivity rather than exotic pairing symmetry. Furthermore, thermal conductivity measurements are consistent with fully gapped superconductivity as there is no linear term at low temperature, and the field dependence suggests multi-band superconductivity [30]. STM [31] and ARPES [32] results support this multi-band picture as they both show multiple relevant bands near the Fermi surface. However, despite this broad agreement, tunnel diode oscillator measurements of the penetration depth were found to be consistent with single-band s-wave superconductivity [33]. This apparent contradiction makes it valuable to perform complementary measurements of the penetration depth to gain additional insight into the superconducting state of PbTaSe<sub>2</sub>.

In this paper we report muon spin rotation and relaxation ( $\mu$ SR) measurements in the superconducting vortex state of PbTaSe<sub>2</sub>. These measurements allow us to extract the temperature dependence of the penetration depth at two different magnetic fields. Zero field  $\mu$ SR measurements also provide a sensitive test for possible time-reversal symmetry breaking in this material. We find weak temperature dependence to the penetration depth at low temperature that can be characterized by fully gapped superconductivity on two bands. Further-

more, we find no evidence for time reversal symmetry breaking.

## EXPERIMENTAL METHODS

The crystal used in this research was prepared by chemical vapor transport at 850 °C using pre-reacted PbTaSe<sub>2</sub>, and PbCl<sub>2</sub> as the transporting agent. Details of the crystal growth can be found in Ref. [34].

Muon spin rotation and relaxation ( $\mu$ SR) experiments were performed at the TRIUMF laboratory in Vancouver, Canada. We used the Pandora dilution refrigerator spectrometer on the M15 surface-muon beam line. This instrument gives access to temperatures between 0.03 K and 10 K with the sample mounted on a silver cold finger, magnetic fields up to 50000 G with a superconducting magnet, and a time resolution of 0.4 ns. The field is applied parallel to the direction of the incoming muon beam, and we performed measurements with the muon spin rotated perpendicular to the field direction. These experiments were performed on a thin crystal aligned with the *c*-axis parallel to the muon beam. We also performed  $\mu$ SR measurements in this cryostat with zero external field using copper coil electromagnets to compensate for ambient magnetic fields. We used the  $\mu$ SRfit software package to analyze the  $\mu$ SR data [35].

Magnetometry measurements were performed at McMaster University using a Quantum Design XL-5 MPMS with an iHelium He<sup>3</sup> cryostat insert for measurements down to 0.5 K. Magnetization curves were measured as a function of temperature on a 3.55 mg single crystal oriented with  $H \parallel c$ -axis. Alignment of the single crystal was verified with Laue X-Ray diffraction prior to the magnetometry and  $\mu$ SR measurements.

## RESULTS AND DISCUSSION

Figure 1 shows the magnetic susceptibility versus temperature of PbTaSe<sub>2</sub> measured in a 10 G field applied parallel to the *c*-axis after cooling in zero field. The susceptibility was calculated by dividing the measured magnetization by the applied field corrected for demagnetizing effects,  $H_{corr} = H - NM$ , where  $N$  is the demagnetizing factor,  $H$  is the applied field, and  $M$  is the magnetization. The crystal we measured had the shape of a thin flat plate with the field applied perpendicular to the plate. We approximate this by an infinitely thin flat sheet, in which case the demagnetizing factor is 1. The susceptibility data shows diamagnetism setting in at low temperatures, indicating a superconducting  $T_C$  of  $3.6 \pm 0.1$  K, in agreement with published data [19]. The sharpness of the transition, occurring over about 0.3 K, shows that our sample is reasonably clean, as chemical or structural disorder would broaden the transition. Furthermore, the strength of the diamagnetic response at low temperature can be used to estimate the superconducting volume fraction, as the suscep-

tibility should be 1 for a pure superconductor at low temperature. We therefore estimate the superconducting volume fraction to be 0.77 which demonstrates that our sample is a bulk superconductor. The small difference from one is likely from partial flux penetration that is expected for a thin superconducting plate, or from uncertainty in the applied field caused by flux trapping in the superconducting magnet. The inset of Figure 1 shows the magnetic moment as a function of applied field at 0.5 K from which we can estimate  $H_{c1} \approx 40$  G and  $H_{c2} \approx 1000$  G.

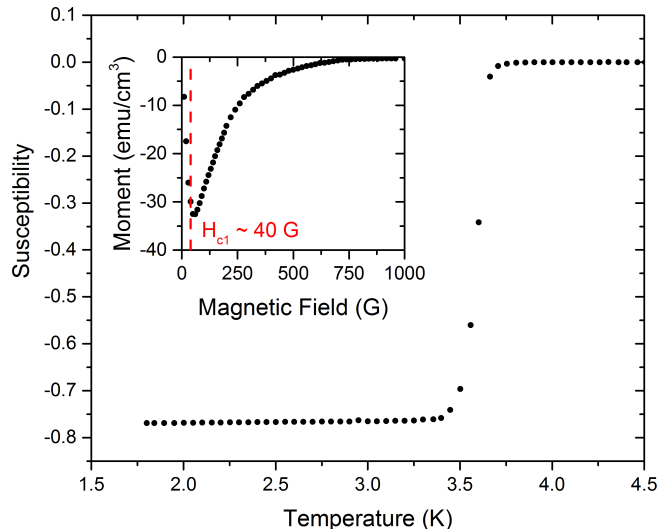


FIG. 1. Magnetic susceptibility measurements on a 3.55 mg single crystal of PbTaSe<sub>2</sub> with a field of 10 G applied parallel to the *c*-axis after cooling in zero field showing a superconducting transition with  $T_C = 3.6$  K. (Inset) Magnetization vs. field measurements at 0.5 K showing a lower critical field  $H_{c1} \approx 40$  G.

Figure 2 (a) shows a  $\mu$ SR asymmetry spectrum collected at 25 mK in a 250 G  $> H_{c1}$  field applied along the *c*-axis of our PbTaSe<sub>2</sub> sample, perpendicular to the muon spin direction. This data shows oscillations as expected for muons precessing in an applied field, while also showing a distinct beat in the amplitude. This demonstrates that there are two components contributing to the asymmetry spectra, as can be seen in the Fourier transform of the asymmetry, shown in Figure 2 (b). In this data, the large peak just below 250 G comes from muons stopping in the silver sample holder or non-superconducting portions of our sample, while the peak at the lower field comes from muons stopping in the superconducting sample. Similarly, the asymmetry spectra in Figure 2 (c) measured at 25 mK in a field of 400 G and the corresponding Fourier transform in Figure 2 (d) also show two oscillating components. At this higher field the superconducting peak is narrower and shifted closer to the silver background peak. This indicates a larger penetration depth and a smaller diamagnetic shift at the higher field. While the Fourier transform data is useful to make qualitative observations, it will always

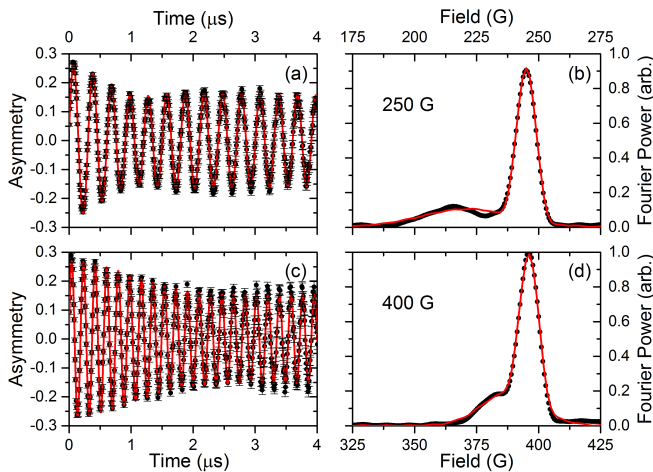


FIG. 2. (a)  $\mu$ SR asymmetry measured at 25 mK in an applied field of 250 G  $\parallel$   $c$ -axis with the muon spins rotated  $\perp$   $c$ -axis. (b) Fourier transform of the data shown in (a). This data shows two peaks, one coming from muons stopping in the superconducting sample and one background peak from muons stopping in the silver sample holder. (c)  $\mu$ SR asymmetry measured at 25 mK in an applied field of 400 G  $\parallel$   $c$ -axis with the muon spins rotated  $\perp$   $c$ -axis. (d) Fourier transform of the data shown in (c). The superconducting peak is wider and shifted closer to the background peak, indicating a larger penetration depth and smaller diamagnetic shift at 400 G compared to 250 G. The red lines in these figures show fits to the data following equation 1.

contain artifacts such as peak broadening caused by the limited time range, and hence we performed all fitting in the time domain.

Muons implanted into a type II superconductor between the lower ( $H_{C1}$ ) and upper ( $H_{C2}$ ) critical fields will see the asymmetric field distribution of the vortex state whose width is related to the London penetration depth ( $\lambda$ ). In our sample  $H_{c1} \approx 40$  G and  $H_{c2} \approx 1000$  G at low temperature, so 250 G and 400 G measurements should both be in the vortex state. However, the small relaxation rate makes it difficult to resolve the field distribution and we mainly see a single peak from the sample in the Fourier transform (in addition to the background silver peak). Furthermore, the large background peak overlaps the field region that we would expect to see the tail of the distribution. These factors make fits to the true vortex lattice field distribution difficult and unreliable. Instead, we fit the superconducting data to a single Gaussian damped oscillating term, where the relaxation rate,  $\sigma_{SC}$ , can be related to the penetration depth, as is commonly done for polycrystalline samples.

We fit the asymmetry data in Figures 2 (a) and (c) with equation 1 and show the fits as the red lines in Figures 2 (a) and (c) and Fourier transformed as the red lines in Figures 2 (b) and (d). This model has two Gaussian damped oscillating terms representing the sample and the silver background. For the fitting, we held the total asymmetry ( $A_T$ ), ratio between components ( $F$ ), silver field ( $B_{Ag}$ ), silver relaxation rate ( $\sigma_{Ag}$ ), and phase ( $\phi$ ) constant while allowing the sample

relaxation rate ( $\sigma_s$ ) and field ( $B_s$ ) to vary and use the constant  $\frac{\gamma_\mu}{2\pi} = 13.5538$  kHz/G for the muon gyromagnetic ratio. The temperature dependence of  $\sigma_s$  and  $B_s$  for both fields is shown in Figure 3. Figure 3 (a) shows an increased in relaxation rate setting in below 2.5 K, while Figure 3 (c) shows a relaxation rate increase below 1.9 K, compared to the measured  $T_C$  of 3.6 K from Figure 1. This is consistent with the expected suppression of  $T_C$  by an applied field for a superconductor with a relatively low  $H_{C2} \approx 1000$  G.

From the sample relaxation rate in Figures 3 (a) and (c), we determined the superconducting component of this relaxation rate by averaging the rate above  $T_C$  to determine a background rate ( $\sigma_{BG}$ ), and then subtracting this off in quadrature from the total rate to give  $\sigma_{SC} = \sqrt{\sigma_s^2 - \sigma_{BG}^2}$ .

$$A = A_T \left[ F \cos(\gamma_\mu B_s t + \phi) e^{-0.5(\sigma_s t)^2} + (1 - F) \cos(\gamma_\mu B_{Ag} t + \phi) e^{-0.5(\sigma_{Ag} t)^2} \right] \quad (1)$$

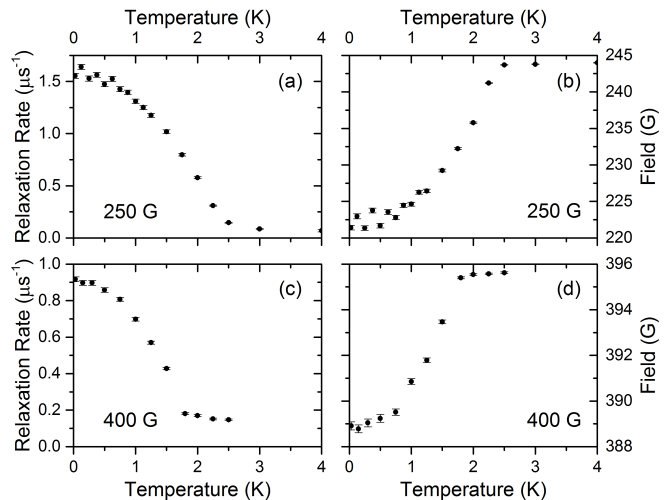


FIG. 3. Fit parameters extracted from fits of the  $\mu$ SR data measured in an applied transverse field to equation 1. (a)  $\sigma_s$  for 250 G applied field. (b)  $B_s$  for 250 G applied field. (c)  $\sigma_s$  for 400 G applied field. (d)  $B_s$  for 400 G applied field.

We can relate the width of the field distribution measured by  $\mu$ SR ( $\sigma_{SC}/\gamma_\mu$ ) with the penetration depth using the relation given by equation 10 in Ref [36]. This equation gives the variance of the magnetic field for an ideal vortex lattice, accurate for the range of applied magnetic fields  $0.25 < B/B_{c2} < 1$ , which is valid for our sample with fields down to 250 G. Expressing  $\lambda$  as a function of  $\sigma_{SC}$  yields:

$$\lambda = \xi \sqrt{(1.94 \times 10^{-2}) \frac{\phi_0}{\xi^2} (1 - b) \frac{\gamma_\mu}{\sigma_{SC}} + 0.069}. \quad (2)$$

Here  $\phi_0 = 2.06783 \times 10^{-15}$  Wb is the flux quantum, and  $\xi$  is the coherence length.

In this equation we used  $H_{c2}$  data from Ref. [30] and the relation  $H_{c2} = \phi_0/(2\pi\xi^2)$  to determine  $\xi$ . The resultant penetration depth is shown in Figure 4. We fit the low temperature penetration depth,  $\lambda$ , with the BCS low temperature limit[37],

$$\lambda(T) = \lambda(0) \left[ 1 + \sqrt{\frac{\pi\Delta_0}{2k_B T}} \exp\left(-\frac{\Delta_0}{k_B T}\right) \right]. \quad (3)$$

Here,  $k_B = 8.617 \times 10^{-5} \text{ eV K}^{-1}$  is Boltzmann's constant,  $T$  is the temperature,  $\Delta_0$  is the zero temperature value of the gap that is allowed to vary and  $\lambda(0)$  is the zero temperature value of the penetration depth that is also allowed to vary. These fits are shown as the solid lines in Figure 4 and show that this model fits the data well. This suggests that the superconducting state is fully gapped without any nodes. From these fits we extract the zero temperature penetration depth values of  $\lambda(0) = 140 \pm 1 \text{ nm}$  at 250 G and  $\lambda(0) = 180 \pm 1 \text{ nm}$  at 400 G.

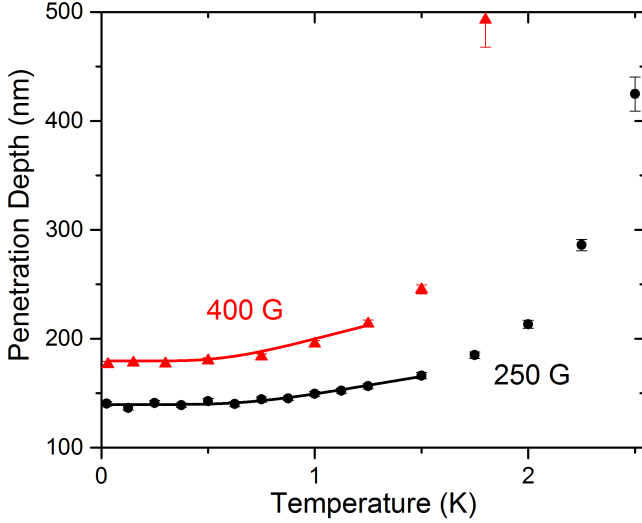


FIG. 4. Penetration depth calculated using equation 2 from the  $\mu$ SR data measured in 250 G (black) and 400 G (red). The solid lines show fits to the data using equation 3 and show that the penetration depth scales as expected for a fully gapped superconductor at low temperature.

As a further test of the pairing symmetry of this material, we calculated the normalized superfluid density as  $n_s/n_0 = \lambda^2(0)/\lambda^2(T)$  for both fields, and show this data in Figure 5. We then used Equation 4 to fit the full temperature range of this data assuming a fully gapped superconductor.

$$\frac{n_s(T)}{n_0} = \left[ 1 - 2 \int_{\Delta}^{\infty} dE \left( -\frac{\partial F}{\partial E} \right) \frac{E}{\sqrt{E^2 - \Delta^2}} \right]. \quad (4)$$

In this equation,  $E$  is the energy difference above the Fermi energy,  $F = \frac{1}{e^{E/k_B T} + 1}$  is the Fermi function, and  $\Delta$  is the

gap, which we approximate using the interpolation formula [39]:

$$\Delta(T) = \Delta_0 \tanh \left( 1.742 \sqrt{\frac{T_c}{T} - 1} \right). \quad (5)$$

To determine the zero temperature value of the gap,  $\Delta_0$ , we use the BCS weak coupling relation,  $\frac{2\Delta_0}{k_B T_c} = 3.5$ . This fit is shown as the solid blue line in Figure 5, where the superfluid density at each field, normalized to the fit zero temperature superfluid density ( $n_0$ ), is plotted against reduced temperature  $T/T_c$ . The values  $T_c(250 \text{ G}) = 2.63 \text{ K}$  and  $T_c(400 \text{ G}) = 2.04 \text{ K}$  were determined from the fit. The fit shows reasonably good agreement at both fields, however there is a small discrepancy at low temperature for the 250 G data where there is an unexplained increase in the superfluid density. A continuing increase in the superfluid density at low temperature is commonly taken to suggest the presence of nodes in the gap [37], however another possibility is multiband superconductivity as has notably been observed in  $\text{MgB}_2$  [40]. For two uncoupled fully gapped bands the superfluid density can be described by the sum, scaled by some weighting factor  $c$ , of the contributions from the different gaps  $\Delta_1$  and  $\Delta_2$  [41],

$$\frac{n_s(T)}{n_0} = c \left[ 1 - 2 \int_{\Delta_1}^{\infty} dE \left( -\frac{\partial F}{\partial E} \right) \frac{E}{\sqrt{E^2 - \Delta_1^2}} \right] + (1 - c) \left[ 1 - 2 \int_{\Delta_2}^{\infty} dE \left( -\frac{\partial F}{\partial E} \right) \frac{E}{\sqrt{E^2 - \Delta_2^2}} \right]. \quad (6)$$

We used this equation to fit the 250 G data and show the fit as the solid green line in Figure 5. This fit gives values of  $c = 0.91$ ,  $\Delta_1 = 0.399 \text{ meV}$  and  $\Delta_2 = 0.109 \text{ meV}$ , suggesting a Fermi surface dominated by a single band, with only a small contribution coming from a second band with smaller gap. The reduced  $\chi^2$  for the two gap fit at 250 G is 1.01 compared to 1.68 for the single band which demonstrates that it is a statistically superior fit. However, we do not see any evidence for a continued increase in the 400 G superfluid density with decreasing temperature as might be expected. This could be explained by the lower gap on the second band: with a lower gap the field required to suppress the superconducting state is expected to be lower which would reduce the influence of multiband behavior at 400 G compared to 250 G.

The increase at low temperature could also be explained by a contribution from a band with an anisotropic gap, such as a d-wave or p-wave component. While our data alone cannot distinguish the isotropic 2-gap state from such a mixed state, comparison with data from other groups makes the fully gapped state most likely. STM measurements show fully gapped superconductivity [31], while thermal conductivity [30] and  $H_{c2}$  [29] are both consistent with multiple fully

gapped bands. This picture also matches the theoretical expectations of Samokhin et al. [18] where a noncentrosymmetric superconductor with pairing caused by phonons should exhibit two-band nodeless superconductivity. PbTaSe<sub>2</sub> has no surrounding magnetic phases that might promote pairing by magnetic fluctuations, and ARPES measurements suggest the role of phonon stiffening in PbTaSe<sub>2</sub> compared to TaSe<sub>2</sub> to explain the appearance of superconductivity [28]. It therefore seems likely that phonon mediated pairing is the mechanism for superconductivity in PbTaSe<sub>2</sub> and thus the model of Samokhin et al. with fully gapped s-wave superconductivity would apply, consistent with our fitting.

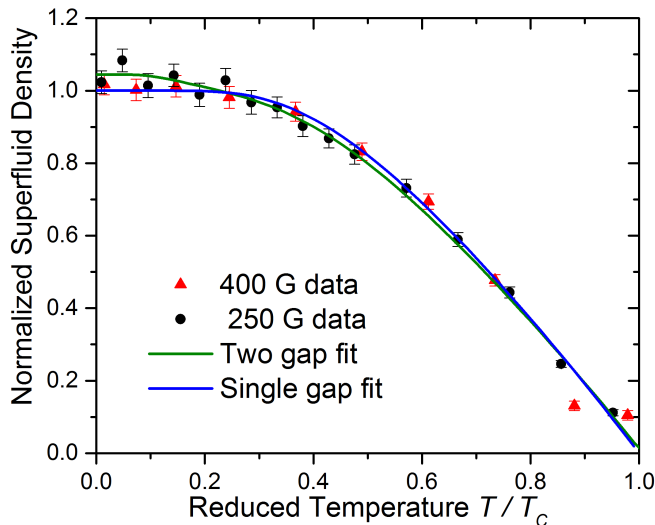


FIG. 5. Normalized superfluid density,  $n_s(T)/n(0)$  plotted versus reduced temperature,  $T/T_C$ , from the 250 G  $\mu$ SR data (black circles) and 400 G  $\mu$ SR data (red triangles). The lines correspond to fits to a single-band model (Equation 4) and a two-band model (Equation 6).

Some pairing symmetries, notably some spin triplet p-wave states, have a spontaneous time reversal symmetry breaking (TRSB) field in the superconducting state. Most TRSB states are characterized by nodes in the gap which are unlikely based on our preceding analysis. However, in high symmetry cubic or hexagonal systems TRSB fields can appear even for fully gapped states [46] as has been recently reported in La<sub>7</sub>Ir<sub>3</sub> [13] and Re<sub>6</sub>Hf [43]. Such fields have in the past been identified by  $\mu$ SR measurements in zero field across the superconducting state [44, 45]. However, as the effect of such a field is very small, significant care must be taken to minimize any stray field at the sample position, lest a relaxation rate change caused by Meissner expulsion of a small field be mistaken for a true time reversal symmetry breaking field.

To perform these careful zero field measurements on our PbTaSe<sub>2</sub> sample following the procedure outlined in Ref. [47], we first loaded a piece of pure silicon in place of the sample and performed measurements at 2 K. At this temperature, a fraction of muons landing in pure silicon bind with

electrons to form muonium, which has a gyromagnetic ratio  $\frac{\gamma_{Mu}}{2\pi} = 1.394 \text{ MHz/G}$ , 103 times larger than that of a bare muon. This gives  $\mu$ SR measurements in low temperature silicon an extremely high sensitivity to small magnetic fields. Figure 6 (a) and (b), which show the asymmetry spectra of silicon at 2 K in a field of 5 G, demonstrate this sensitivity. Figure 6 (a) shows the early time spectra with the fast oscillations coming from muonium. Figure 6 (b) shows the asymmetry out to 8 ms and shows the fast oscillations coming from muonium as well as the slower oscillations coming from bare muons. This data is fit with two oscillating components given by equation 7, where the field,  $B$ , is the same for both components,  $F_{Mu} = 0.16$  is the muonium fraction,  $\lambda_{Mu}$  and  $\lambda_\mu$  are the muonium and muon signal relaxation rates, and  $\phi_{Mu}$  and  $\phi_\mu$  are phase offsets for the muonium and muon components.

$$A = A_T \left[ F_{Mu} \cos(\gamma_{Mu} B t + \phi_{Mu}) e^{-(\lambda_{Mu} t)} + (1 - F_{Mu}) \cos(\gamma_\mu B t + \phi_\mu) e^{-(\lambda_\mu t)} \right] \quad (7)$$

Using this silicon sample, we zeroed the field by adjusting the currents in copper coil electromagnets arranged in three perpendicular directions. In this procedure, we measured spectra with the muon spin parallel and perpendicular to the beam momentum, ensuring that the field in all directions was minimized. Figures 6 (c) and (d) show the silicon spectra at 2 K after performing this zeroing procedure with the muon spins in both possible orientations. No oscillations are observed in this data, and the field fits to a value of  $0_{-0}^{+0.3}$  G indicating that a good zero field condition was produced.

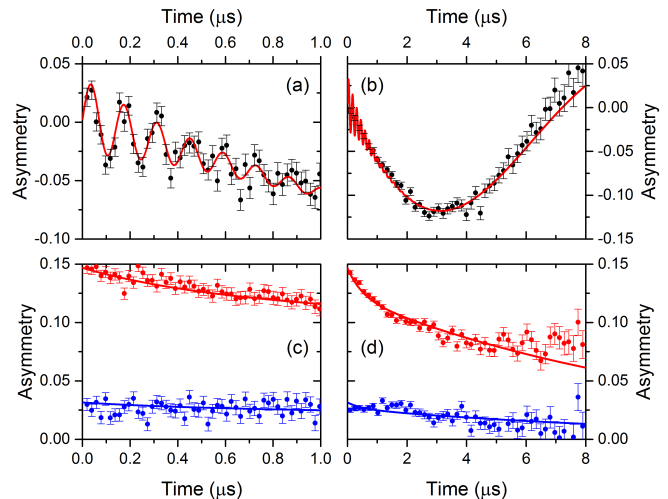


FIG. 6. (a) Example silicon muonium asymmetry spectra at early times in an external field of 5 G. (b) Silicon asymmetry at long times in an external field of 5 G. (c) Early time silicon asymmetry after zeroing the field. Red shows data with the muon spins parallel to momentum, and blue with the muon spins rotated perpendicular to the momentum. (d) Late time spectra corresponding to (c).

Once we arrived at this zero field condition, we re-loaded

the PbTaSe<sub>2</sub> single crystal sample in place of the silicon and performed zero field  $\mu$ SR measurements with the muon spins parallel to the c-axis. Figure 7 shows this data for representative temperatures between 0.025 and 5 K. The asymmetry in this figure represents the signal coming only from the sample. The background signal coming from muons stopping in the silver sample holder is time-independent and we have allowed the baseline shift parameter ( $\alpha$ ), commonly used in  $\mu$ SR to account for varying detector efficiencies and geometric effects, to also account for the baseline shift caused by the silver background. This results in a total asymmetry which is comparable to the sample component of the transverse field measurements. The relaxation of this asymmetry in zero field will come from nuclear magnetic moments or from electronic magnetism. As the nuclear moments will not be much affected by temperature, and there are no known structural transitions which would modify the muon stopping site, any significant change in the relaxation rate with temperature is expected to signal the onset of electronic magnetism.

Figure 7 shows no visible difference between the asymmetry spectra at all temperatures. Fitting the data to a single exponentially relaxing component,  $A = A_T e^{-\lambda t}$ , we extract the relaxation rate ( $\lambda$ ) and plot it in Figure 7 (b). This figure shows no significant change in relaxation rate down to 0.025 K. To estimate an upper limit on the internal field of the sample, we fit Figure 7 (b) to a mean field order parameter, approximated by Equation 8:

$$\lambda = c \tanh \left( 1.742 \sqrt{\frac{T_c}{T} - 1} \right) + \lambda_0. \quad (8)$$

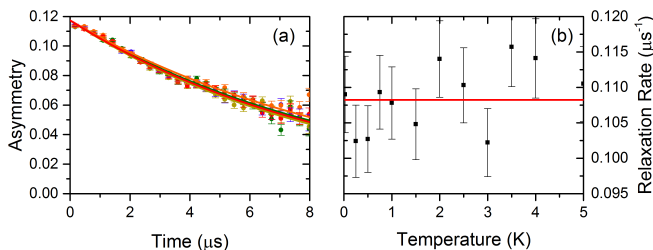


FIG. 7. (a)  $\mu$ SR asymmetry measured in zero applied field at 0.025 K (blue), 1 K (green), 2 K (yellow), 3 K (orange), and 5K (red). (b) Fit relaxation rate for  $\mu$ SR data measured in zero field. The red line shows a fit to a mean field order parameter with  $T_C = 3.6$  K approximated by Equation 8.

Here  $\lambda$  is the relaxation rate,  $\lambda_0$  is a background relaxation rate,  $c$  is the order parameter, and  $T_C$  is fixed at 3.6 K. The fit yields  $c = 0 \pm 0.004 \mu s^{-1}$ , which gives an upper limit on the internal field of 0.05 G. Typical stray fields for time reversal symmetry breaking in triplet superconductors are between 0.1 and 0.5 G [44, 48], substantially larger than our upper limit. We therefore suggest that there is no time reversal

symmetry breaking in PbTaSe<sub>2</sub> coming from triplet pairing. In certain non-centrosymmetric systems, smaller TRSB fields of around 0.08 G [13, 43] have been reported in fully gapped superconducting states. These fields are still larger than our fitting limit, but we cannot rule out a slightly smaller TRSB field existing in our system.

## CONCLUSION

Our results suggest that PbTaSe<sub>2</sub> is not purely a conventional s-wave superconductor as the superfluid density is not flat at low temperatures. Zero field  $\mu$ SR measurements find no evidence for a TRSB field, and are of sufficient precision to rule out the field magnitudes seen in other noncentrosymmetric and centrosymmetric superconductors. These features are overall consistent with describing PbTaSe<sub>2</sub> as a multi-band superconductor, with isotropic fully-gapped superconductivity existing on both bands.

## ACKNOWLEDGMENTS

We thank G.D. Morris, B.S. Hitti and D.J. Arseneau for their assistance with the  $\mu$ SR measurements. Work at McMaster University was supported by the Natural Sciences and Engineering Research Council of Canada and the Canadian Foundation for Innovation. M.N.W acknowledges support from the Alexander Graham Bell Canada Graduate Scholarship program. The Columbia University group acknowledges support from NSF DMR-1436095 (DMREF), NSF DMR-1610633, OISE-0968226 (PIRE), JAEA Reimei project, and Friends of Univ. of Tokyo Inc. F.C.C. acknowledges support funded by the Ministry of Science and Technology (MOST), Taiwan under Project No. 103-2119-M-002-020-MY3.

- [1] E. Bauer and M. Sigrist. *Non-centrosymmetric Superconductors* (2012)
- [2] N. Hayashi, K. Wakabayashi, P.A. Frigeri and M. Sigrist. *Physical Review B* **73**, 024504 (2006)
- [3] M. Sigrist, D.F. Agterberg, P.A. Frigeri, N. Hayashi, R.P. Kaur, A. Koga, I. Milat, K. Wakabayashi and Y. Yanase. *Journal of Magnetism and Magnetic Materials* **310** 536 (2007)
- [4] T. Takimoto and P. Thalmeier. *Journal of the Physical Society of Japan* **78** 103703 (2009)
- [5] I. Bonalde, W. Brámer-Escamilla and E. Bauer. *Physical Review Letters* **94**, 207002 (2005)
- [6] H. Mukuda, T. Fujii, T. Ohara, A. Harada, M. Yashima, Y. Kitaoka, Y. Okuda, R. Settai and Y. Onuki. *Physical Review Letters* **100**, 107003 (2008)
- [7] I. Bonalde, R.L. Ribeiro, W. Bramer-Escamilla, G. Mu and H.H. Wen. *Physical Review B* **79**, 052506 (2009)
- [8] E. Bauer, G. Rogl, X.-Q. Chen, R.T. Khan, H. Michor, G. Hilscher, E. Royanian, K. Kumagai, D.Z. Li, Y.Y. Li, R. Podloucky and P. Rogl. *Physical Review B* **82**, 064511 (2010)
- [9] M. Nishiyama, Y. Inada and G.-q. Zheng. *Physical Review Letters* **98**, 047002 (2007)
- [10] H.Q. Yuan, D.F. Agterberg, N. Hayashi, P. Badica, D. Vandervelde, K. Togano, M. Sigrist and M.B. Salamon. *Physical Review Letters* **97**, 017006 (2006)
- [11] M. Isobe, M. Arai and N. Shirakawa. *Physical Review B* **93**, 054519 (2016)
- [12] V.K. Anand, A.D. Hillier, D.T. Adroja, A.M. Strydom, H. Michor, K.A. McEwen and B.D. Rainford. *Physical Review B* **83**, 064522 (2011)
- [13] J.A.T. Barker, D. Singh, A. Thamizhavel, A.D. Hillier, M.R. Lees, G. Balakrishnan, D. McK. Paul and R.P. Singh. *Physical Review Letters* **115**, 267001 (2015)
- [14] A.D. Hillier, J. Quintanilla and R. Cywinski. *Physical Review Letters* **102**, 117007 (2009)
- [15] Y. Iwamoto, Y. Iwasaki, K. Ueda and T. Kohara. *Physics Letters A* **250**, 439 (1998)
- [16] H.Q. Yuan, D.F. Agterberg, N. Hayashi, P. Badica, D. Vandervelde, K. Togano, M. Sigrist and M.B. Salamon. *Physical Review Letters* **97**, 017006 (2006)
- [17] K. Sugawara, T. Sato, S. Souma, T. Takahashi and A. Ochiai. *Physical Review B* **76**, 132512 (2007)
- [18] K.V. Samokhin and V.P. Mineev. *Physical Review B* **77**, 104520 (2008)
- [19] M.N. Ali, Q.D. Gibson, T. Klimczuk and R.J. Cava. *Physical Review B* **89**, 020505(R) (2014)
- [20] L. Fang, Y. Wang, P.Y. Zou, L. Tang, Z. Xu, H. Chen, C. Dong, L. Shan and H.H. Wen. *Physical Review B* **72**, 014534 (2005)
- [21] R. Morosan, H.W. Zandbergen, B.S. Dennis, J.W.G. Bos, Y. Onose, T. Klimczuk, A.P. Ramirez, N.P. Ong and R.J. Cava. *Nature Physics* **2**, 544 (2006)
- [22] T. Yokoya, T. Kiss, A. Chainani, S. Shin, M. Nohara and H. Takagi. *Science* **294**, 2518 (2001)
- [23] A.F. Kusmartseva, B. Sipos, H. Berger, L. Forró and E. Tutiš. *Physical Review Letters* **103**, 236401 (2009)
- [24] J.J. Yang, Y. J. Choi, Y.S. Oh, A. Hogan, Y. Horibe, K. Kim, B.I. Min and S-W. Cheong. *Physical Review Letters* **108**, 116402 (2012)
- [25] B. Sipos, A.F. Kusmartseva, A. Akrap, H. Berger, L. Forró. *Nature Materials* **7**, 960 (2008)
- [26] K. Horiba, K. Ono, J.H. Oh, T. Kihara, S. Nakazono, M. Oshima, O. Shiino, H.W. Yeom, A. Kakizaki and Y. Aiura. *Physical Review B* **66**, 073106 (2002)
- [27] A. Aharafiev, R. Sankar, A. Glamazada, K.-Y. Choi, R. Bohle, P. Lemmens and F. Chou. *arXiv:1505.00748* (2015)
- [28] T.-R. Chang, P.-J. Chen, G. Bian, S.-M. Huang, H. Zheng, T. Neupert, R. Sankar, S.-Y. Xu, I. Belopolski, G. Chang, B.K. Wang, F. Chou, A. Bansil, H.-T. Jeng, H. Lin and M.Z. Hasan. *Physical Review B* **93**, 245130 (2016)
- [29] J. Wang, X. Xu, N. Zhou, Li, X. Cao, J. Yang, Y. Li, C. Cao, J. Dai, J. Zhang, Z. Shi, B. Chen and Z. Yang. *J Supercond Nov Magn* **28**, 3173 (2015)
- [30] M.X. Wang, Y. Xu, L.P. He, J. Zhang, X.C. Hong, P.L. Cai, Z.B. Wang, J.K. Dong and S.Y. Li. *Physical Review B* **93**, 020503(R) (2016)
- [31] S.-Y. Guan, P.-J. Chen, M.-W. Chu, R. Sankar, F. Chou, H.-T. Jeng, C.-S. Chang and T.-M. Chuang. *Science Advances* **2**, e1600894 (2016)
- [32] G. Bian, T.-R. Chang, R. Sankar, S.-Y. Xu, H. Zhang, T. Neupert, C.-K. Chiu, S.-M. Huang, G. Chang, I. Belopolski, D.S. Sanchez, M. Neupane, N. Alidoust, C. Lie, B.K. Wang, C.-C. Lee, H.-T. Jeng, C. Zhang, Z. Yuan, S. Jia, A. Bansil, F. Chou, H. Lin and M. Z. Hasan. *Nature Communications* **7**, 10556 (2016)
- [33] G.M. Pang, M. Smidman, L.X. Zhao, Y.F. Wang, Z.F. Weng, L.Q. Che, Y. Chen, X. Lu, G.F. Chen and H.Q. Yuan. *Physical Review B* **93**, 060506(R) (2016)
- [34] R. Sankar, G.S. Rao, I.P. Muthuselvam, T.-R. Chang, H.T. Jeng, G.S. Murugan, W.-L. Lee and F.C. Chou. *J. Phys. Condens. Matter* **29**, 095601 (2017)
- [35] A. Suter and B.M. Wojek. *Physics Procedia* **30**, 69 (2012)
- [36] E.H. Brandt. *Physical Review B* **68**, 054506 (2003)
- [37] R. Prozorov, and R.W. Giannetta. *Supercond. Sci. Technol.* **19**, R41 (2006)
- [38] S.K. Yip and J.A. Sauls. *Physical Review Letters* **69**, 2264 (1992)
- [39] F. Gross, B.S. Chandrasekhar, D. Einzel, K. Andres, P.J. Hirschfeld, H.R. Ott, J. Beuers, Z. Fisk and J.L. Smith. *Zeitschrift für Physik B* **64**, 175 (1986)
- [40] A.A. Golubov, A. Brinkman, O.V. Dolgov, J. Kortus and O. Jepsen. *Physical Review B* **66**, 054524 (2002)
- [41] M.-S. Kim, J.A. Skinta, T.R. Lemberger, W.N. Kang, H.-J. Kim, E.-M. Choi and S.-I. Lee. *Physical Review B* **66**, 064511 (2002)
- [42] G. Bian, T.-R. Chang, R. Sankar, S.-Y. Xu, H. Zheng, T. Neupert, C.-K. Chiu, S.-M. Huang, G. Chang, I. Belopolski, D.S. Sanchez, M. Neupane, N. Alidoust, C. Liu, B. Wang, C.-C. Lee, H.-T. Jeng, C. Zhang, Z. Yuan, S. Jia, A. Bansil, F. Chou, H. Lin and M.Z. Hasan. *Nature Communications* **7**, 10556 (2015)
- [43] R.P. Singh, A.D. Hillier, B. Mazidian, J. Quintanilla, J.F. Annett, D. McK. Paul, G. Balakrishnan, M.R. Lees. *Physical Review Letters* **112**, 107002 (2014)
- [44] G.M. Luke, Y. Fudamoto, K.M. Kojima, M.I. Larkin, J. Merrin, B. Nachumi, Y.J. Uemura, Y. Maeno, Z. Q. Mao, Y. Mori, H. Nakamura and M. Sigrist. *Nature* **394**, 558 (1998)
- [45] M. Smidman, M.B. Salamon, H.Q. Yuan and D.F. Agterberg. *Reports on Progress in Physics* **80**, 036501 (2017)
- [46] D.F. Agterberg, V. Barzykin and L.P. Gor'kov. *Physical Review B* **60**, 14868 (1999)
- [47] G.D. Morris and R.F. Heffner. *Physica B* **326**, 252 (2003)
- [48] G.M. Luke, A. Keren, L.P. Le, W.D. Wu, Y.J. Uemura, D.A. Bonn, L. Taillefer and J.D. Garrett. *Physical Review Letters* **71**, 1466 (1993)